

# Travelling-Wave Excitation for 16.4T Small-Bore MRI

Patrick Bluem<sup>1</sup>, Alexey Tonyushkin<sup>2</sup>, Dinesh Deelchand<sup>3</sup>, Gregor Adriany<sup>3</sup>, Pierre-Francois Van de Moortele<sup>3</sup>, Andrew J M Kiruluta<sup>2</sup>, Zoya Popovic<sup>1</sup>

<sup>1</sup>University of Colorado, Boulder, Colorado

<sup>2</sup>Massachusetts General Hospital, Harvard Medical School, Boston, Massachusetts

<sup>3</sup>University of Minnesota Medical School, Minneapolis, Minnesota

**Abstract** — In this paper, we present the design of a probe for a travelling-wave 16.4T small-bore animal research MRI system. The probe is a 698-MHz coaxially-fed microstrip patch designed to give a circularly polarized magnetic field when placed in the bore cavity. Images of a water phantom using the patch probe are obtained and compared with simulations. Additionally, a periodic axial strip cylinder is inserted into the bore, resulting in a 7-fold increase in SNR, and enabling both gradient recalled echo and spin echo imaging of the phantom. The modified mode content in the image is compared to full-wave simulations.

**Index Terms** — Magnetic Resonance Imaging, waveguide, travelling-wave, patch, circular polarization.

## I. INTRODUCTION

In clinical 1.5T and 3T magnetic resonance imaging (MRI) instruments, the object being imaged is closely coupled to the detector through near fields and detection is performed through Faraday probes [1,2]. Nuclear magnetic resonance (NMR) can also be excited and detected using long-range coupling with travelling waves, demonstrated by several research groups over the past few years, e.g. [3]. One benefit of this approach is more uniform coverage of samples that are larger than the wavelength of the NMR signal. Uniform spatial coverage in MRI is traditionally achieved by tailoring the reactive near field of resonant Faraday probes. This approach is valid when the radio-frequency wavelength at the Larmor frequency is substantially larger than the target volume, which does not hold for modern, wide-bore, high-field systems.

This paper addresses a new method of integrated design of exposure and excitation of UHF and low microwave frequency magnetic fields for next-generation MRI at high magnetic flux densities ( $B_0 > 3$  T) [4-6], which improve the signal-to-noise ratio (SNR) [7]. For example, at 7 T, the required RF frequency is 298 MHz range, while a bore that fits a human is at least 60 cm in diameter, making it above the cutoff frequency for at least one mode of the bore viewed as a waveguide, when the waveguide is loaded with tissues which have high dielectric constants. The travelling waves can potentially be advantageous in terms of a more comfortable environment for patients, larger field of view, imaging hard to reach organs (e.g., prostate gland) and some areas that were until now inaccessible to MRI (e.g., inner ear), as well as enabling new spatial encoding schemes and a variety of mode sensitivity profiles [8].

To date, a few pre-clinical human scanners at 7T and 9.4T [3,9] and small bore research (animal) 16T and 21.1T [10] systems were used to demonstrate traveling-wave (TW) MRI. Whole-body scanner dimensions result in the bore being an above cut-off cylindrical waveguide with one or two TW modes propagating in the unloaded bore. In contrast, most of the small-bore research, as well as clinical (<4T) systems, do not support traveling waves unless high dielectric inserts [11] or coaxial transmission lines [12] for mode propagation. Typical RF probes for preclinical TW-MRI are electric dipole probes or standard patch antennas that couple energy to the loaded waveguide modes, with the goal of providing as uniform as possible circularly polarized B-field inside the dielectric to be imaged [13].

In this paper, we present the design of a travelling-wave probe for a 16.4 T small-bore MRI system, some bore modifications which enable increased SNR, and finally measured data on a water phantom obtained in the setup shown in Figure 1.

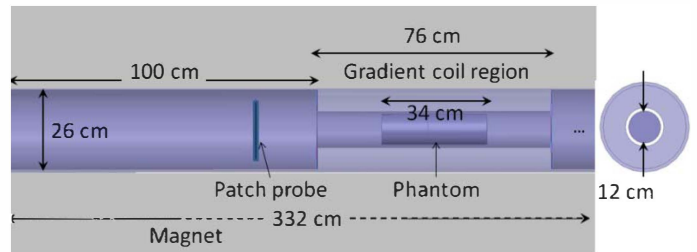


Fig. 1. Sketch of 16.4T small bore Varrian MRI with relevant dimensions and position of phantom shown. The traveling wave probe position can be varied inside the wider cylinder to demonstrate exposure and detection without near-field coupling. The entire magnet length is not shown for clarity, the total length being 3.32m.

## II. EXPERIMENTAL SETUP

The small-bore setup sketch in Fig.1 shows the relevant dimensions and the position of the water phantom and patch probe. The total length of the 16.4 T superconducting magnet and bore is 332cm, not drawn to scale in Fig.1. The gradient coil part of the bore is smaller in diameter than the outer part, the diameters being 12cm and 26 cm, respectively. The larger cylindrical portion to the left where the probe is placed is 100cm long, and a similar 138-cm long portion is to the right

of the gradient coil region. The inside wall of the bore is insulated. The water phantom is 34cm long and fits snugly in the smaller cylindrical part of the bore. The probe can be translated through the bore, which results in a change in matching, as well as variations in the excitation field in the phantom. It is fed by 3 kW of power at the Larmor frequency of 698 MHz.

### III. PROBE DESIGN

The probe designed for the 16.4-T bore from Fig.1 is a circular single-coaxial feed slotted patch. The probe is designed using full-wave simulations (Ansoft HFSS), with the bore and phantoms taken into account. The phantom is simulated as a uniform dielectric cylinder with  $\epsilon_r=81$  and a conductivity of  $10^{-4}$ S/m. The substrate is an FR4 62.5-mil thick double-sided copper printed circuit board. The patch feed is a single coaxial input as shown in Fig.2, and the two 5-mm wide slots in the ground plane are 6.85 and 7.1cm long and excite circularly-polarized waves [14].

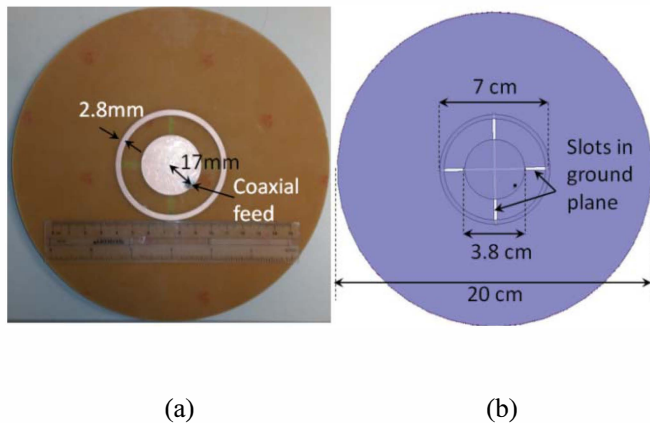


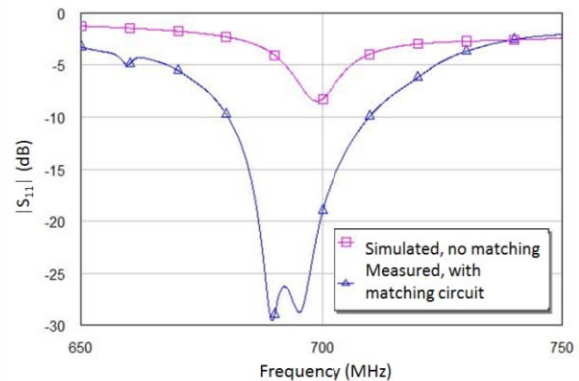
Fig. 2. Photograph (a) and layout (b) of circularly-polarized patch probe with a single coaxial feed and two slots in the ground plane that ensure circular polarization.

The measured and simulated return loss, calibrated to the coaxial feed reference plane, is shown in Fig.3. The patch itself had about 8dB return loss, so a narrowband microstrip matching circuit is designed to obtain a return loss greater than 20dB when the probe is placed in the bore.

Note that although some antenna theory and approaches are used in the design of the patch, it is not actually an antenna in free space, but rather a probe that couples to modes in the loaded bore waveguide. Therefore, the simulations are done inside a metal cylinder the size of the bore, and the distance to the gradient coil portion is varied to verify the traveling wave conditions. Coupling of the circularly-polarized field into the phantom is also examined in simulations by observing the transverse components of the B-field.



(a)



(b)

Fig. 3. (a) Photo of patch probe placed 50 cm into the bore. (b) Simulated return loss of the patch probe when placed inside the bore without a matching circuit (red) and measured return loss in the bore with an electrically short high-impedance line microstrip matching circuit connected between the coaxial cable and patch feed point.

### IV. 16.4-T MRI IMAGES

The phantom used for the experiments is a dielectric acrylic tube ( $L=34$  cm,  $D=9$  cm) filled with deionized water or saline. With the patch probe placed 50cm into the bore, as in Fig.3a, MR images consistent with simulated B-field are obtained and are shown in Figure 4.

In order to improve the SNR, A cylindrical array of 3-cm wide longitudinal copper strips 2-m long and 12cm in diameter is inserted in the bore with a goal of modifying the travelling-wave mode content in the gradient coil region, as shown in Figure 5. The longitudinal strips present an artificial electromagnetic surface and modify the boundary conditions of the metallic bore. Since they are oriented in the axial direction, the strips present a different surface impedance to the axial electric field than to the transverse field, thus modifying the mode profile. This can be seen in both simulations and measurements of the axial cross-section shown in Figure 6(a). The coronal images are in good agreement with field simulations as shown in Figure 6(b). For these images, the patch probe is placed 5cm from the edge of the bore at the start of the strip cylinder. The MR images were obtained with a GRE sequence: FOV=20x20 cm, TR/TE=275ms/2.1ms, slice thickness of 1 mm for both axial and coronal slices. The high spatial frequency fringes and

edge brightening correspond to artifacts due to unencoded volume of the dielectric guide that extends beyond the gradient insert.

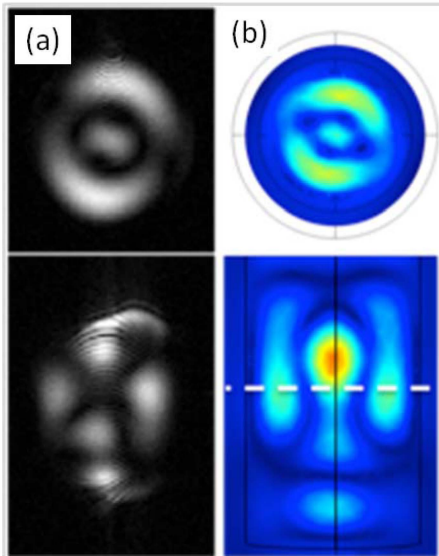


Fig. 4. (a) Measured axial (top) and sagittal (bottom) cross-sections inside the phantom. (b) Normalized simulated circularly polarized B-field for the sagittal and axial cuts, using COMSOL Multiphysics.

In order to improve the SNR, A cylindrical array of 3-cm wide longitudinal copper strips 2-m long and 12cm in diameter is inserted in the bore with a goal of modifying the travelling-wave mode content in the gradient coil region, as shown in Figure 5.

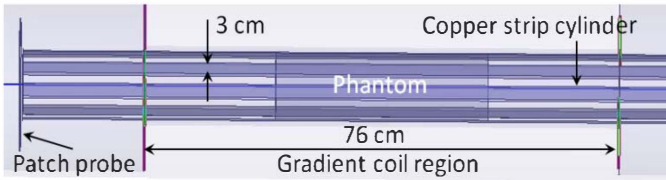


Fig. 5. Sketch of parallel copper strip cylinder inserted into the bore and extending beyond the gradient coil region by 5cm. The patch probe is placed at the beginning of the cylinder.

The longitudinal strips present an artificial electromagnetic surface and modify the boundary conditions of the metallic bore. Since they are oriented in the axial direction, the strips present a different surface impedance to the axial electric field than to the transverse field, thus modifying the mode profile. This can be seen in both simulations and measurements of the axial cross-section shown in Figure 6(a). The coronal images are in good agreement with field simulations as shown in Figure 6(b). For these images, the patch probe is placed 5cm from the edge of the bore at the start of the strip cylinder. The MR images were obtained with a GRE sequence: FOV=20x20 cm, TR/TE=275ms/2.1ms, slice thickness of 1 mm for both axial and coronal slices. The high spatial frequency fringes

and edge brightening correspond to artifacts due to unencoded volume of the dielectric guide that extends beyond the gradient insert.

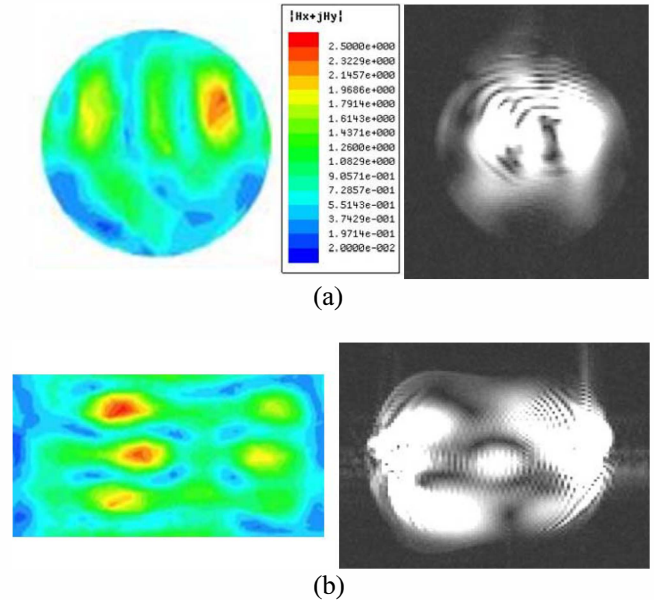


Fig. 6. Magnitude of the simulated transverse right handed circular-polarized H-Field normalized to 1W power input at the SMA connector of the probe (left) and MR images (right) taken with the patch probe and metal strip cylinder inserted in the bore, at a specific cross-section of the phantom for (a) axial and (b) coronal cross-sections. The SNR is increased seven-fold compared to the images in Fig.4.

## V. CONCLUSIONS AND DISCUSSION

The circular patch probe was chosen after an investigation of other possible probes that result in similar magnetic field profiles in the phantom. A rectangular patch probe was also investigated with dimensions shown in Fig.7 and designed on the same type of substrate as the circular patch probe, resulting in a return loss of 18dB when simulated inside the bore.

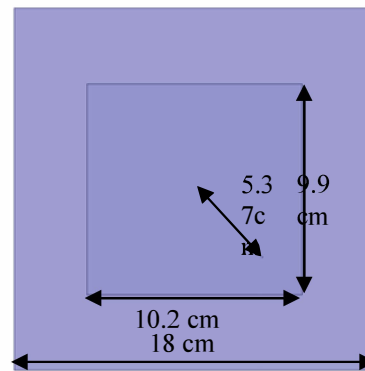


Fig. 7. Layout of circularly-polarized rectangular patch with a single coaxial feed in the lower right.

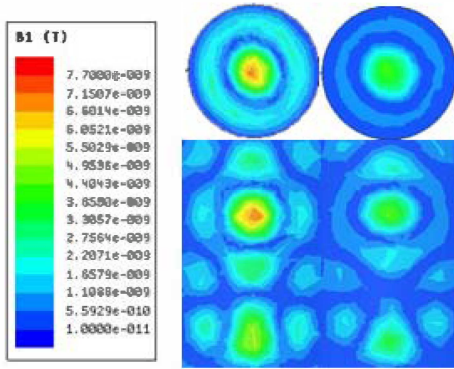


Fig. 8. Magnitude of the transverse right handed circular-polarized B-field normalized to 1W power input at the SMA connector of the probe for axial (top) and sagittal (bottom) simulated for the circular patch (left) and the rectangular patch (right) in HFSS. These images do not perfectly match the experimental image of Fig. 4 due to the MR image being a result of both polarizations.

Figure 8 shows a comparison of the simulated magnetic field inside the phantom for the two probes. The simulations are performed for similar conditions as in the experiment. The simulations imply that the magnetic field profile is relatively independent of the type of probe that is chosen, as waveguide theory suggests. However, the location of the probe will influence the field distribution. The rectangular probe has a disadvantage because of its size, and the reduced size of the circular probe is a result of significant design efforts. In contrast to the rectangular patch probe, the circular probe is small enough and can fit in the gradient coil portion of the bore, and can also be scaled to fit inside 3T, 7T and 10T static field MRI systems.

In summary, this paper demonstrates 16.4T MR images in a phantom excited by a travelling-wave field patch probe far from the phantom. In addition, an anisotropic copper strip cylinder is inserted into the bore, modifying the modal content. Although the guide diameter is too small to support traveling waves above cut-off for a metal guide, the strip cylinder changes the boundary condition thus changing the mode cutoff frequencies, allowing TW MRI, with a *seven-fold increase in SNR* as compared to the patch probe without the strip cylinder. Due to the high SNR, in addition to GRE, we were able to obtain spin-echo images, with an example shown in Fig.9. These results demonstrate that traveling wave MRI with high SNR can be performed with proper probe exciters and bore design when the bore is small compared to the free-space wavelength of the Larmor frequency.

## VI. ACKNOWLEDGEMENTS

The authors acknowledge support by the National Science Foundation under a collaborative research grant ECCS 1307614 at the University of Colorado, Boulder.

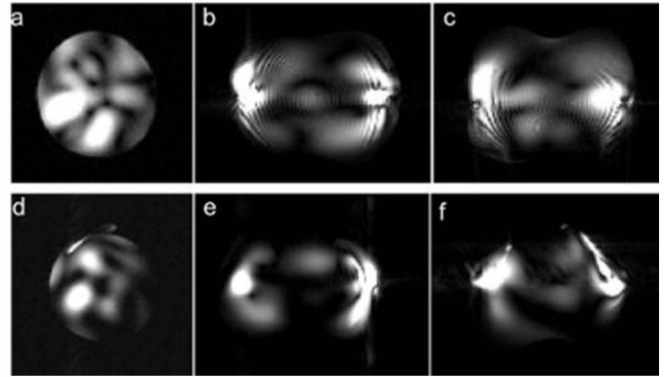


Fig. 9. GRE (a-c) and SE (d-f) images obtained in phantom with patch and metal strip cylinder: (a,d) axial, (b,e) coronal, and (c,f) sagittal slices. (SE parameters: TR/TE=1s/20ms, FOV=20x20 cm, matrix=256x128, slice thickness of 2 mm, 0.8 mm gap, 10 slices).

## REFERENCES

- [1] P.B. Roemer, *et al.* "The NMR phased array," *Magn. Reson. Med.* 16, 192–225 (1990).
- [2] J.T. Vaughan, *et al.* "High frequency volume coils for clinical NMR imaging and spectroscopy," *Magn. Reson. Med.* 32, 206–218 (1994).
- [3] D. O. Brunner, *et al.* "Travelling-wave nuclear magnetic resonance," *Nature* 457(7232). 994-U2. 2009.
- [4] R. Fu, *et al.* "Ultra-wide bore 900 mhz high-resolution nmr at the national high magnetic field laboratory,," *Journal of Magnetic Resonance* 177 (2005) 1–8.
- [5] V. D. Schepkin, *et al.* "In vivo Rodent Sodium and Proton MR Imaging at 21 T," *Magn. Reson. Imaging*, 28(3). 400-7. 2010.
- [6] A. G. Webb, *et al.* "MRI and localized proton spectroscopy in human leg muscle at 7 tesla using longitudinal traveling waves," *Magnetic Reson. Med.*, 63 (2010) 297–302.
- [7] K. Haines, *et al.* "Microimaging with a Cylindrical Ceramic Dielectric Resonator at 21.1 T," *Proc. Exp. NMR Conf.* 2010.
- [8] A.J.M. Kiruluta, "The emergence of the propagation wave vector in high field NMR: analysis and implications," *J. Physics D-Applied Physics*, 40(10). 3043-3050. 2007.
- [9] F. H. Geschewski, *et al.*, "Optimum coupling and multimode excitation of traveling-waves in a whole-body 9.4T scanner," *Magn. Reson. Med.*, vol. 69, no. 6, pp.1805-1812, June, 2013.
- [10] A. Tonyushkin, *et al.*, "Traveling Wave MRI in a Vertical Bore 21.1-T System," *Intern. Magn. Reson. Med.*, Melbourne, 2012.
- [11] A. Tonyushkin, *et al.*, "Imaging with Dielectric Waveguide Approach for 3T MRI," *Intern. Soc. Magn. Reson. Med.*, Melbourne, 2012.
- [12] J. A. Tang, *et al.*, "Cutoff-free traveling wave NMR," *Concepts in Magnetic Resonance Part A*, vol. 38A, no. 5, pp.253-267, September, 2011.
- [13] A.J.E. Raaijmakers, *et al.*, "Design of a radiative surface coil array element at 7T: The single-side adapted dipole antenna," *Magn. Reson. Med.*, vol. 66, pp.1488-1497, November 2011.
- [14] X.L. Biao, M.J. Ammann, *IET Electronic Lett.*, Vol.42, No.4, Feb. 2006.